Acta Crystallographica Section F
Structural Biology Communications
ISSN 2053-230X

Structural mechanism of DNA recognition by the p202 HINa domain: insights into the inhibition of Aim2-mediated inflammatory signalling

He Li, Jue Wang, Jie Wang, Lu-Sha Cao, Zhi-Xin Wang and Jia-Wei Wu*

MOE Key Laboratory of Protein Science and Tsinghua–Peking Center for Life Sciences, School of Life Sciences, Tsinghua University, Beijing 100084, People's Republic of China

Correspondence e-mail: jiaweiwu@mail.tsinghua.edu.cn

Received 21 August 2013
Accepted 15 November 2013

PDB reference: p202 HINa domain, 4lnq

The HIN-200 family of proteins play significant roles in inflammation-related processes. Among them, AIM2 (absent in melanoma 2) and IFI16 (γ-interferon-inducible protein 16) recognize double-stranded DNA to initiate inflammatory responses. In contrast, p202, a mouse interferon-inducible protein containing two HIN domains (HINa and HINb), has been reported to inhibit Aim2-mediated inflammatory signalling in mouse. To understand the inhibitory mechanism, the crystal structure of the p202 HINa domain in complex with a 20 bp DNA was determined, in which p202 HINa nonspecifically recognizes both strands of DNA through electrostatic attraction. The p202 HINa domain binds DNA more tightly than does AIM2 HIN, and the DNA-binding mode of p202 HINa is different from that of the AIM2 HIN and IFI16 HINb domains. These results, together with the reported data on p202 HINb, lead to an interaction model for full-length p202 and dsDNA which provides a conceivable mechanism for the negative regulation of Aim2 inflammasome activation by p202.

1. Introduction

The innate immune system is the first line of defence against infection by foreign organisms and recognizes pathogens in a nonspecific manner (Akira *et al.*, 2006). Nucleic acids, the major macromolecules for life, are potent triggers of the innate immune response. Recently, a number of RNA/DNA-recognizing receptors have been reported (Barbalat *et al.*, 2011). Among the diverse DNA receptors, human AIM2 (absent in melanoma 2) and IFI16 (γ-interferon-inducible protein 16) are both members of the HIN-200 protein family (haematopoietic interferon-inducible nuclear proteins containing a 200-amino-acid signature repeat; Dawson & Trapani, 1996).

The structurally and functionally related HIN-200 family comprises four human members and 14 verified or putative murine proteins (Ludlow *et al.*, 2005), and most of them contain two types of functional domains: a pyrin domain (PYD) at the N-terminus and one or two copies of the signature HIN domain at the C-terminus (Schattgen & Fitzgerald, 2011; Hornung *et al.*, 2009). The PYD domain adopts the death-domain fold, which has been identified in many proteins involved in inflammation-related or apoptosis-related processes (Park, 2012). The death domains are evolutionarily conserved and comprise an antiparallel α-helical bundle. The PYD domains of the HIN-200 proteins engage in homotypic protein–protein interactions to form large complexes (Kersse *et al.*, 2011; Park *et al.*, 2007), and their HIN domains can mediate DNA binding and/or protein–protein interaction (Ludlow *et al.*, 2005; Schattgen & Fitzgerald, 2011). For instance, the HIN domain of AIM2 interacts with cytoplasmic DNA and its PYD domain binds to the adaptor protein ASC (apoptosis-associated speck-like protein containing a caspase-recruitment domain). ASC can further recruit the effector enzyme procaspase-1, resulting in the formation of the large signalling complex inflammasome and the activation of inflammatory responses

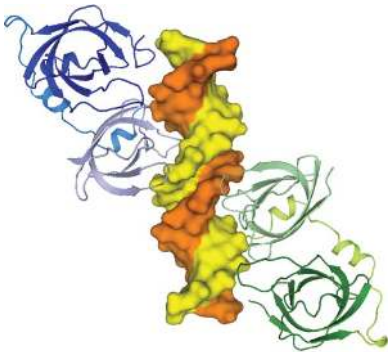

(Fernandes-Alnemri *et al.*, 2009; Bürckstümmer *et al.*, 2009; Hornung *et al.*, 2009; Roberts *et al.*, 2009). Therefore, AIM2 has been shown to play significant roles in host defence against pathogens such as *Streptococcus pneumoniae*, *Listeria monocytogenes*, *Francisella tularensis*, *Legionella pneumophila* and *Mycobacterium tuberculosis* (Rathinam *et al.*, 2010; Saiga *et al.*, 2012; Kim *et al.*, 2010; Tsuchiya *et al.*, 2010; Sauer *et al.*, 2010; Fernandes-Alnemri *et al.*, 2010; Jones *et al.*, 2010; Ge *et al.*, 2012; Fang *et al.*, 2011). However, high levels of AIM2 and cytosolic DNA have also been found in several inflammatory skin diseases (de Koning *et al.*, 2012; Dombrowski *et al.*, 2011). In contrast, IFI16 consists of one PYD and two HIN domains (HINa and HINb), and has been linked to the formation of the caspase-1-activating inflammasome in the nucleus in response to Kaposi's sarcoma-associated herpesvirus (Kerur *et al.*, 2011).

The mouse interferon-inducible protein p202 is distinct from other HIN-200 proteins in that it contains only two HIN domains (HINa and HINb) and no PYD domain and has no identified human homologues (Ludlow *et al.*, 2005). Owing to the lack of the PYD domain, p202 cannot bind to ASC *via* the homotypic PYD–PYD interaction and is incapable of stimulating inflammatory signalling. However, p202 has been demonstrated to bind DNA efficiently (Choubey & Gutterman, 1996) and also to interact with mouse Aim2 (in the following, Aim2 refers to the mouse protein and AIM2 denotes the human protein) in cytosol (Choubey *et al.*, 2000). These properties have recently been linked to the inhibitory effect of p202 on Aim2 inflammasome activation (Roberts *et al.*, 2009). However, the molecular mechanism by which p202 represses Aim2-dependent inflammatory signalling remains elusive.

Recently, structural studies have validated the existence of two oligonucleotide/oligosaccharide-binding (OB) fold subdomains within each HIN domain and have revealed the molecular mechanisms of DNA recognition by the HIN domains of AIM2, IFI16 and p202 (Jin *et al.*, 2012; Yin *et al.*, 2013; Ru *et al.*, 2013; Liao *et al.*, 2011). Here, we determined the crystal structure of the p202 HINa domain in complex with 20 bp double-stranded DNA, in which two p202 HINa molecules bind tandemly to the major groove of dsDNA. The p202 HINa domain binds DNA in a different manner from the HIN domains of AIM2/Aim2 and IFI16. Using these results and reported biochemical and structural data, we propose a conceivable model for the interaction of full-length p202 with dsDNA, which sheds light on the inhibitory role of p202 on Aim2 function.

2. Materials and methods

2.1. Protein preparation

The human AIM2 DNA template was synthesized by Generay Biotech Co. Ltd, Shanghai and the mouse p202 and Aim2 cDNAs were gifts from Dr Xu Zhao. The human AIM2 HIN domain (141–343), mouse Aim2 HIN domain (141–345) and mouse p202 HINa domain (52–248) were respectively inserted into a vector derived from pETDuet-1 (Novagen), which contains a 3C protease cleavage site after the N-terminal His_6 tag. The site-specific mutations of the mouse p202 HINa domain were generated using site-directed mutagenesis. All constructs were authenticated by DNA sequencing.

All HIN-domain proteins were overexpressed in *Escherichia coli* JM109 (DE3) cells. The cells were grown in Luria–Bertani medium at 37°C to an $OD_{600\ nm}$ of 0.8. The expression of recombinant protein was then induced with IPTG at a final concentration of 1 m*M* at 18°C for 16 h. The cells were harvested by centrifugation at 2500*g* and the cell pellets were resuspended in purification buffer (50 m*M* Tris–HCl pH 8.0, 300 m*M* NaCl) supplemented with 10 m*M* $MgCl_2$, 200 U ml^{-1} DNaseI and 1 m*M* PMSF. The cells were lysed by sonication and the lysate was centrifuged at 20 000*g* for 45 min. The His_6-tag fusion proteins in the supernatant were bound to Ni–NTA agarose (Qiagen) pre-equilibrated with the purification buffer. The Ni–NTA beads were washed with the purification buffer supplemented with 10 m*M* imidazole and then desalted with 50 m*M* Tris–HCl pH 8.0. The His_6-tagged HIN protein was eluted using purification buffer supplemented with 250 m*M* imidazole. The proteins were then subjected to cation-exchange chromatography (Source 15S, GE Healthcare) eluted with a 0–500 m*M* NaCl gradient in 50 m*M* Tris–HCl pH 8.0. Fractions containing the HIN protein were collected and the His_6 tag was removed by incubation with 1 µ*M* 3C protease at 4°C overnight. The completeness of the protein digestion was checked by SDS–PAGE and no His_6-tagged protein was detected in the overnight mixture. The mixture was diluted approximately fivefold with 50 m*M* Tris–HCl pH 8.0 and was further purified *via* a second Source 15S run to remove the free His_6 tag and 3C protease. The eluted untagged HIN proteins were concentrated using Amicon stirred cells (EMD Millipore) and were then subjected to size-exclusion chromatography (Superdex 200 10/300 GL, GE Healthcare) in a buffer consisting of 10 m*M* Tris–HCl pH 8.0, 150 m*M* NaCl, 2 m*M* DTT. The proteins were stored at −80°C and their purity was greater than 95% as judged by SDS–PAGE.

Table 1
Data-collection and refinement statistics.

The data set was collected from a single crystal. Values in parentheses are for the highest resolution shell.

Data collection	
Space group	$P2_12_12$
Unit-cell parameters (Å, °)	a = 95.4, b = 105.6, c = 65.1, $\alpha = \beta = \gamma = 90$
Resolution (Å)	40.0–2.0 (2.07–2.00)
No. of unique reflections	44832
Multiplicity	7.8 (7.9)
Completeness (%)	99.7 (99.7)
$\langle I/\sigma(I)\rangle$	27.4 (4.4)
R_{merge} (%)	9.6 (63.4)
Refinement	
Resolution (Å)	36.15–2.00 (2.05–2.00)
R_{work}/R_{free} (%)	20.00/23.4 (25.8/31.9)
No. of atoms	
Protein	3123
DNA	814
Water	327
Average B factors (Å^2)	
Wilson B factor	32.0
Protein	40.8
DNA	54.3
Water	43.3
R.m.s. deviations	
Bond lengths (Å)	0.008
Bond angles (°)	1.12
Ramachandran plot analysis	
Favoured	371 [96.9%]
Allowed	12 [3.1%]
Disallowed	0 [0%]

2.2. DNA-binding analysis

The unlabelled DNA oligonucleotide (5′-CCATCAAAGATCTT-TGATGG-3′ without 5′-phosphate) was synthesized by Invitrogen (People's Republic of China) and the 5′-fluorescein (FAM) labelled DNA oligonucleotide was synthesized by Sangon Biotech Shanghai Co. Ltd. The oligonucleotides were dissolved in a buffer consisting of 10 m*M* Tris–HCl pH 8.0, 150 m*M* NaCl, 2 m*M* DL-dithiothreitol and annealed as reported by Jin *et al.* (2012). Binding of the HIN domains to dsDNA was determined by a fluorescence polarization (FP) assay (Jin *et al.*, 2012). The 5′-FAM-labelled dsDNA (15 n*M*) was mixed

with different HIN proteins at the indicated concentrations. The mixtures were aliquoted into black 384-well plates in triplicate, and the fluorescence polarization was measured using an EnVision Multilabel Plate Reader (Perkin Elmer).

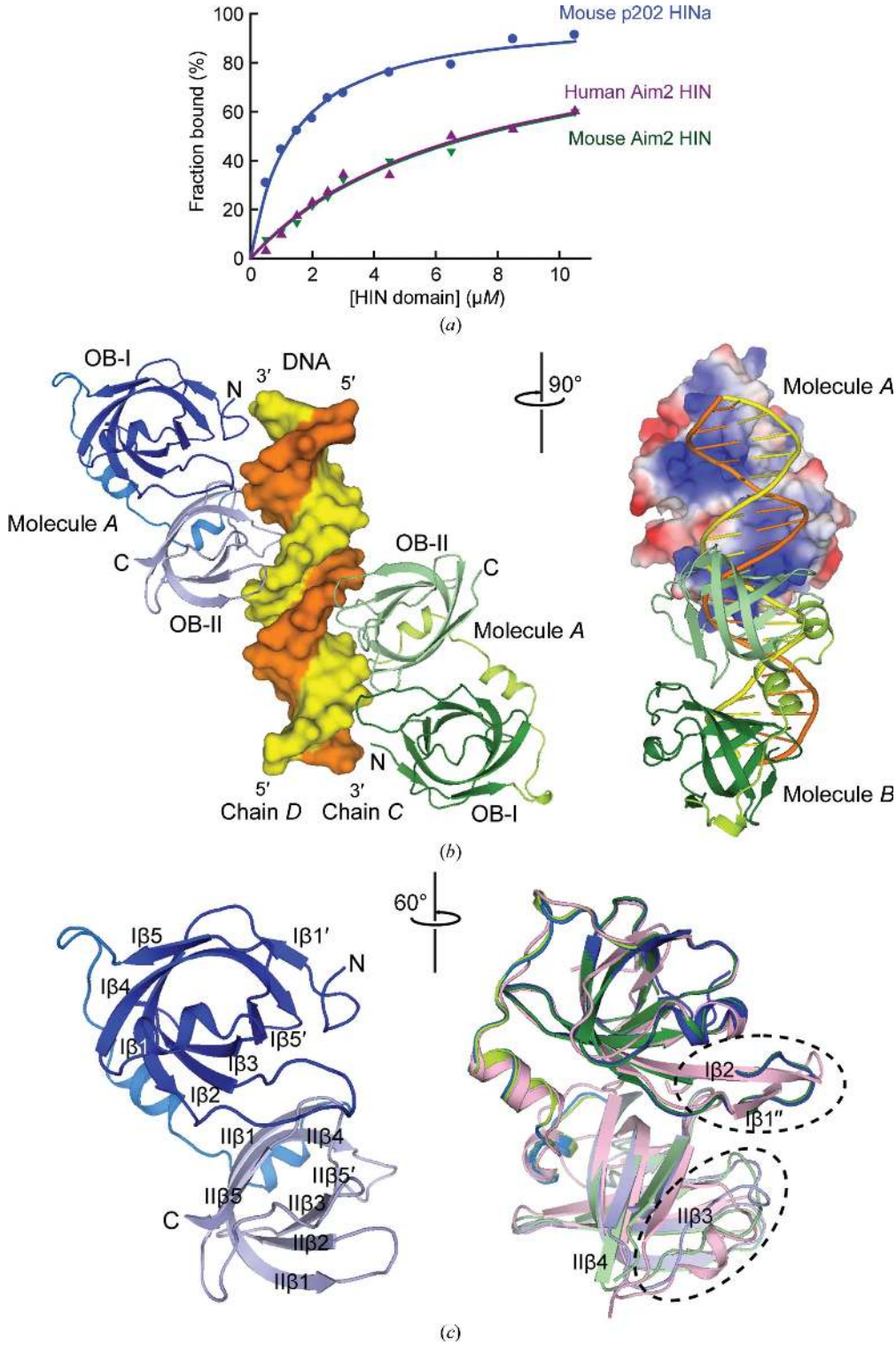

Figure 1
Structure of mouse p202 HINa bound to dsDNA. (*a*) Fluorescence polarization assays of the FAM-labelled dsDNA binding to mouse p202 HINa, mouse Aim2 HIN and human AIM2 HIN. The assays were performed in the presence of 15 n*M* 5′-FAM-labelled dsDNA and the indicated HIN proteins at various concentrations. (*b*) Graphical representations of the p202 HINa domain in complex with a 20 bp dsDNA in two views related by a 90° rotation around a vertical axis. Molecule *A* and molecule *B* of p202 HINa within the asymmetric unit are coloured blue and green, respectively, and chain *C* and chain *D* of dsDNA are shown in orange and yellow, respectively. In the left panel, the locations of the N-termini and C-termini of the two p202 HINa molecules are marked, and the dsDNA is shown as a surface model. In the right panel, molecule *A* is shown as surface representation coloured according to electrostatic potential (positive, blue; negative, red). (*c*) Ribbon representations of p202 HINa in two views related by a 60° rotation around a vertical axis. All β-strands are labelled in the left panel, and a structural comparison of two p202 HINa molecules with the human AIM2 HIN domain (coloured pink; PDB entry 3rn2) is shown on the right.

2.3. Crystallography

The p202 HINa domain protein (2.13 m*M*) and the unlabelled 20 bp dsDNA (0.5 m*M*) were both in buffer consisting of 10 m*M* Tris–HCl pH 8.0, 150 m*M* NaCl, 2 m*M* DTT. The protein–DNA complex for crystallization trials was prepared by mixing the protein (65 µl) and dsDNA (138.5 µl) to give a final molar ratio of 2:1 (680 µ*M* protein:340 µ*M* dsDNA) and the mixture was then incubated at 4°C for 30 min for full equilibration. Crystals were grown using the hanging-drop vapour-diffusion method by mixing the protein–DNA complex with an equal volume of reservoir solution consisting of 0.1 *M* bis-tris pH 5.5, 0.2 *M* ammonium acetate, 10 m*M* strontium chloride, 17% PEG 3350 at 294 K. The crystals were cryoprotected in reservoir solution supplemented with 20% glycerol and were flash-cooled in a cold nitrogen stream at 100 K. A diffraction data set was collected to 2.0 Å resolution on beamline 17U at the Shanghai Synchrotron Radiation Facility (SSRF; Shanghai, People's Republic of China) and processed using the *HKL*-2000 package (Otwinowski & Minor, 1997). The structure was initially solved by molecular replacement using *Phaser* (McCoy *et al.*, 2007; Winn *et al.*, 2011) with

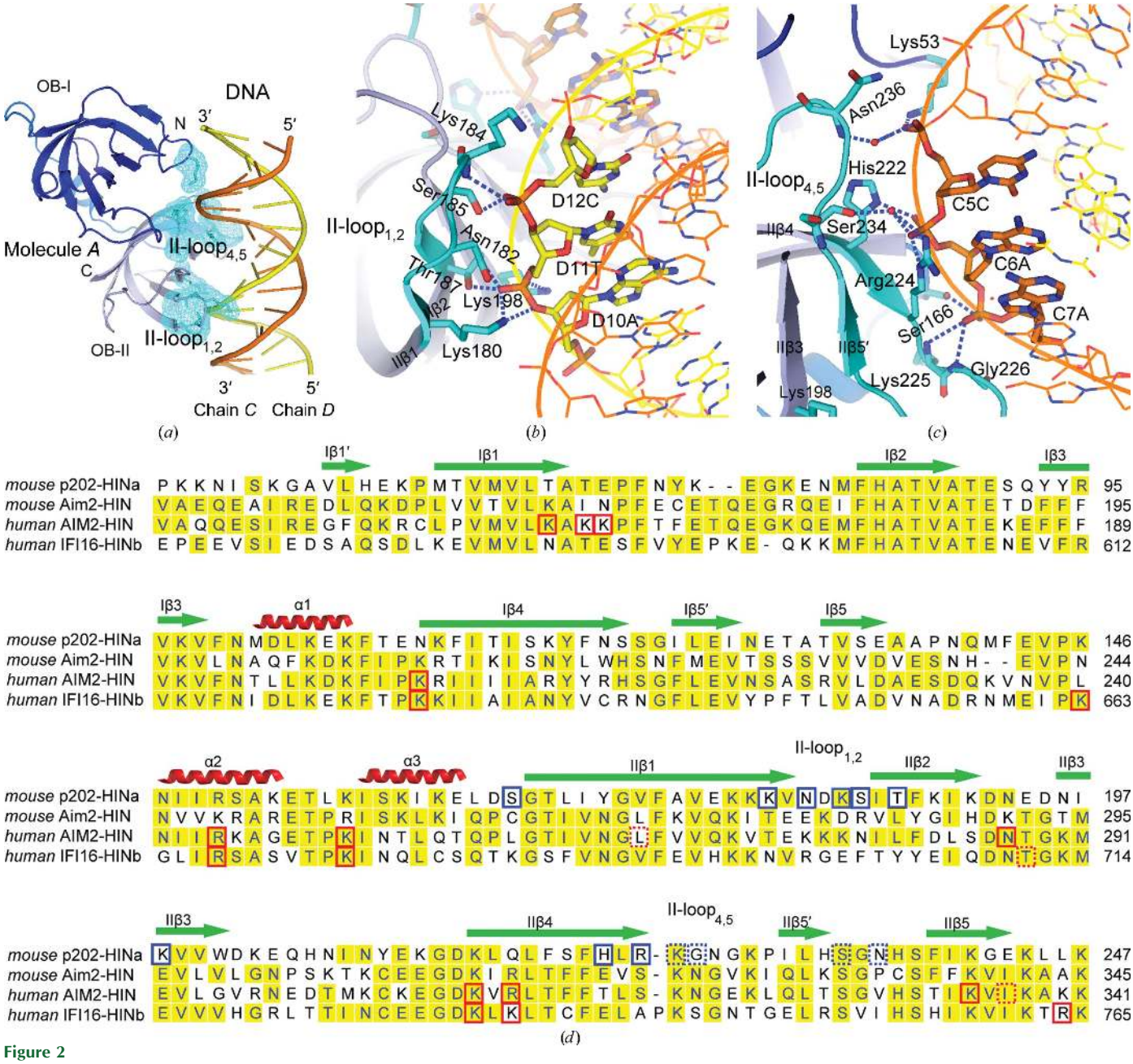

Figure 2
p202 HINa recognizes dsDNA in a nonspecific manner. (*a*) Two loop regions of p202 HINa bind to the major groove of dsDNA. Residues interacting with dsDNA are shown as a cyan mesh. (*b*, *c*) Detailed interactions between the II-loop$_{1,2}$ region (*b*) and the II-loop$_{4,5}$ region (*c*) of p202 HINa and dsDNA. Residues involved in DNA binding are highlighted as cyan sticks and the II-loop$_{1,2}$ region is also coloured cyan. The water molecules mediating the protein–DNA interaction are shown as red balls. (*d*) Sequence alignment of mouse p202 HINa (SwissProt entry Q9R002), mouse Aim2 HIN (Q91VJ1), human AIM2 HIN (O14862) and human IFI16 HINb (Q16666). The secondary-structure elements defined in p202 HINa are shown at the top of the alignment. The residues of p202 HINa involved in the interaction with dsDNA are boxed in blue and those of human AIM2 HIN and IFI16 HINb are boxed in red. The solid boxes indicate interactions involving side chains from the HIN domains, and the dotted boxes indicate main-chain interactions.

the DNA-free IFI16 HINb structure (PDB entry 3b6y, chain *A*, approximately 40% identity to p202 HINa) as the search model. The best solution showed that there are two HIN-domain molecules in the asymmetric unit (RFZ = 8.5, TFZ = 7.9, LLG = 99 and RFZ = 4.8, TFZ = 28.1, LLG = 634). The ideal dsDNA was manually fitted to the strong electron density indicative of a DNA duplex in *Coot* (Emsley & Cowtan, 2004). Further refinement was performed with *PHENIX* (Adams *et al.*, 2010) and *Coot*. There are two p202 HINa molecules per asymmetric unit, with an r.m.s. deviation of 0.4 Å for 161 C^{α} atoms. Model quality was assessed with *Coot* during rebuilding and with *PROCHECK* (Laskowski *et al.*, 1993). All residues were in the allowed regions of the Ramachandran plot, as defined by *MolProbity* (Chen *et al.*, 2010), with 96.9% of the residues in the most favoured regions. Data-processing and refinement statistics are summarized in Table 1. All structural representations were prepared with *PyMOL* (http://www.pymol.org). The atomic coordinates and structure factors have been deposited in the Protein Data Bank as entry 4lnq.

3. Results and discussion

3.1. Structure of p202 HINa bound to dsDNA

To determine how p202 regulates the Aim2 signalling pathway, we purified recombinant mouse p202 HINa, human AIM2 HIN and mouse Aim2 HIN domain proteins. We first performed a fluorescence polarization (FP) assay to investigate *in vitro* interactions between these HIN domains and 5′-FAM-labelled double-stranded DNA (dsDNA). The HINa domain of p202 interacts with dsDNA in a dose-dependent manner, similar to the AIM2/Aim2 HIN domains (Fig. 1*a*). The K_d value for the mouse p202 HINa domain was determined to be 1.33 ± 0.11 μ*M*, approximately fivefold lower than those for the human AIM2 HIN domain (7.29 ± 0.99 μ*M*) and the mouse Aim2 HIN domain (7.10 ± 1.37 μ*M*). To elucidate the molecular basis of the tighter DNA recognition by p202, we determined the crystal structure of p202 HINa in complex with a 20 bp dsDNA to 2.0 Å resolution (Table 1). Within an asymmetric unit, two p202 HINa molecules (chains *A* and *B*) bind to the major groove of dsDNA (chains *C* and *D*), which adopts the regular B-form (Fig. 1*b*). The protein–DNA recognition mainly involves positively charged residues on the p202 HINa surface and the nonesterified phosphate O atoms from both strands of the dsDNA, in a similar way to that observed in the AIM2 HIN–DNA and IFI16 HINb–DNA complexes (Jin *et al.*, 2012). However, the DNA-binding mode of p202 HIN is highly distinct from the reported HIN–DNA interaction (see below).

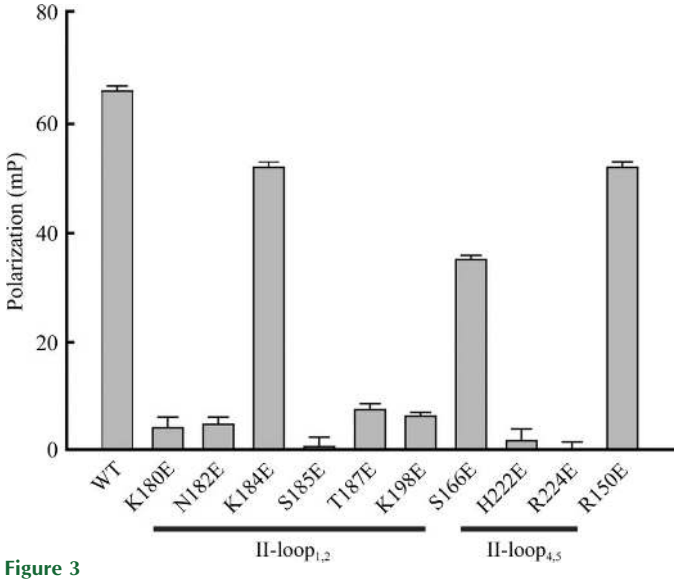

Figure 3
Effects of mutations at the interface of p202 HINa on the dsDNA-binding ability. Fluorescence polarization assays were performed to determine the DNA-bound fractions of the wild-type and mutant proteins (mean and standard error, n = 3). The assays were performed in the presence of 10 μ*M* p202 HINa protein and 15 n*M* 5′-FAM-labelled dsDNA.

The two p202 HINa molecules adopt essentially the same conformation, with an overall r.m.s. deviation of 0.4 Å for 161 C^{α} atoms (Fig. 1*c*). Very recently, two structural studies of p202 were independently reported (Ru *et al.*, 2013; Yin *et al.*, 2013), and the p202 HINa domains in these protein–dsDNA complexes (PDB entries 4jbk, 4l5r and 4l5s) adopt almost identical conformations as our p202 HINa structure, with comparable r.m.s. deviations to that of our two p202 HINa molecules within the asymmetric unit. The p202 HINa structure is similar to the reported structures of AIM2 HIN (PDB entry 3rn2; r.m.s.d of 1.47 Å over 166 C^{α} atoms), IFI16 HINa (PDB entry 2oq0; r.m.s.d of 0.89 Å over 165 C^{α} atoms) and IFI16 HINb (PDB entry 3b6y; r.m.s.d of 1.09 Å over 150 C^{α} atoms) (Jin *et al.*, 2012; Liao *et al.*, 2011).

The p202 HINa domain comprises two canonical OB folds (OB-I and OB-II), which are connected by a linker containing two α-helices. Each OB fold mainly consists of a β-barrel of five strands (β1–β5) and the strands are marked 'I' and 'II' for OB-I and OB-II, respectively, in the left panel of Fig. 1(*c*). The major structural deviations of these HIN structures are mapped to several loops. For instance, in the first OB fold (OB-I), the connection between strands Iβ1 and Iβ2 of p202 HINa is more flexible than that in the AIM2 HIN domain because the OB-I fold of p202 HINa lacks strand Iβ1′ and its strand Iβ2 is shorter (Fig. 1*c*, right panel). In addition, the loops connecting the β-strands in the second OB fold (OB-II) vary significantly, in particular the loop between strands IIβ3 and IIβ4.

3.2. Nonspecific interactions between p202 HINa and dsDNA

The two p202 HINa domains within the asymmetric unit bind to the major groove of dsDNA in the same manner, each resulting in the burial of approximately ∼1370 $Å^2$ of exposed surface area. The structural analyses in the following were on the basis of the dsDNA and molecule *A* of p202 HINa, which had lower average temperature factors (39.0 $Å^2$ for molecule *A* and 42.6 $Å^2$ for molecule *B*). Intriguingly, an overwhelming majority of the DNA-binding residues are located on the surface of the OB-II fold, while the connection linker and the OB-I fold contribute very little to DNA association (Fig. 2*a*). The OB-II fold interacts with both backbones of the dsDNA through two respective regions. One interface mainly involves residues from the loop between strands IIβ1 and IIβ2 (the II-loop$_{1,2}$) and two sequential nucleotides on chain *D* of the dsDNA (Fig. 2*b*). For instance, the phosphate of nucleotide D11T forms multiple hydrogen bonds to the basic or polar side chains of Lys180, Asn182 and Thr187 within the II-loop$_{1,2}$ and Lys198 on strand IIβ3, and the phosphate of the adjacent D12C binds to the side-chain hydroxyl group of Ser185 and the main-chain amide group of Lys184. The other interface is centred at the II-loop$_{4,5}$ between strands IIβ4 and IIβ5 (Fig. 2*c*). The main-chain amide groups of Lys225 and Gly226 in II-loop$_{4,5}$, as well as the hydroxyl group of Ser166 N-terminal to strand IIβ1, interact with the phosphate of nucleotide C7A, and the basic side chains of His222 and Arg224 at the N-terminus of strand IIβ4 coordinate the backbone of C6A. In addition to these direct protein–DNA interactions, Ser234 and Asn236 N-terminal to strand IIβ5 form water-mediated hydrogen bonds to the phosphate groups of C6A and C5C, respectively. The only interaction involving the OB-I subdomain is

formed between the extreme N-terminal residue Lys53 and the phosphate group of C5C (Fig. 2*c*). Overall, the p202 HINa domain binds DNA nonspecifically through hydrophilic interactions between two loop regions in the OB-II subdomain and the backbone phosphate groups on both strands of dsDNA, and no specific π–π stacking involving DNA bases was observed (Fig. 2*d*).

To assess the interactions between p202 HINa and dsDNA, we generated a series of point mutations (mutated to Glu) located in the p202 HINa OB-II interface, and their effects on DNA-binding ability were examined using a fluorescence polarization (FP) assay (Fig. 3). A majority of the mutations in the II-loop$_{1,2}$ region (K180E, N182E, S185E, T187E and K198E) completely abolished the dsDNA-binding ability of the p202 HINa domain, while substituting Lys184, a residue located on the edge of the II-loop$_{1,2}$ interface and interacting with DNA *via* its main chain, had little effect. In addition, individually mutating the II-loop$_{4,5}$ residues His222 and Arg224 to Glu dramatically reduced the protein–DNA interactions, whereas the S166E mutant partially impaired the DNA-binding ability. We also mutated Arg150 on the concave surface of p202 HINa because the corresponding residues of AIM2 HIN and IFI16 HINb are both involved in HIN–DNA interactions (Fig. 2*d*). As expected, the R150E mutation did not affect the DNA binding of p202 HINa. These data clearly demonstrate that the two loop regions in the OB-II fold, but not the concave surface involving both OB folds, are indispensable for interaction of the p202 HINa domain with dsDNA.

3.3. p202 HINa and AIM2 HIN bind double-stranded DNA in different modes

It has been reported that the human AIM2 HIN, mouse Aim2 HIN and human IFI16 HINb domains exhibit the same binding mode for dsDNA *via* nonspecific interactions (Jin *et al.*, 2012; Sung *et al.*, 2012). To our surprise, when the AIM2 HIN domain and p202 HINa domain were positioned in the same orientation, the dsDNA molecules unexpectedly bound to different sides of the HIN domains and were almost perpendicular to each other (Fig. 4). The p202 HINa molecule binds alongside the dsDNA, mainly through the II-loop$_{1,2}$ and II-loop$_{4,5}$ regions in the second OB fold (Fig. 4*a*, left panel). The

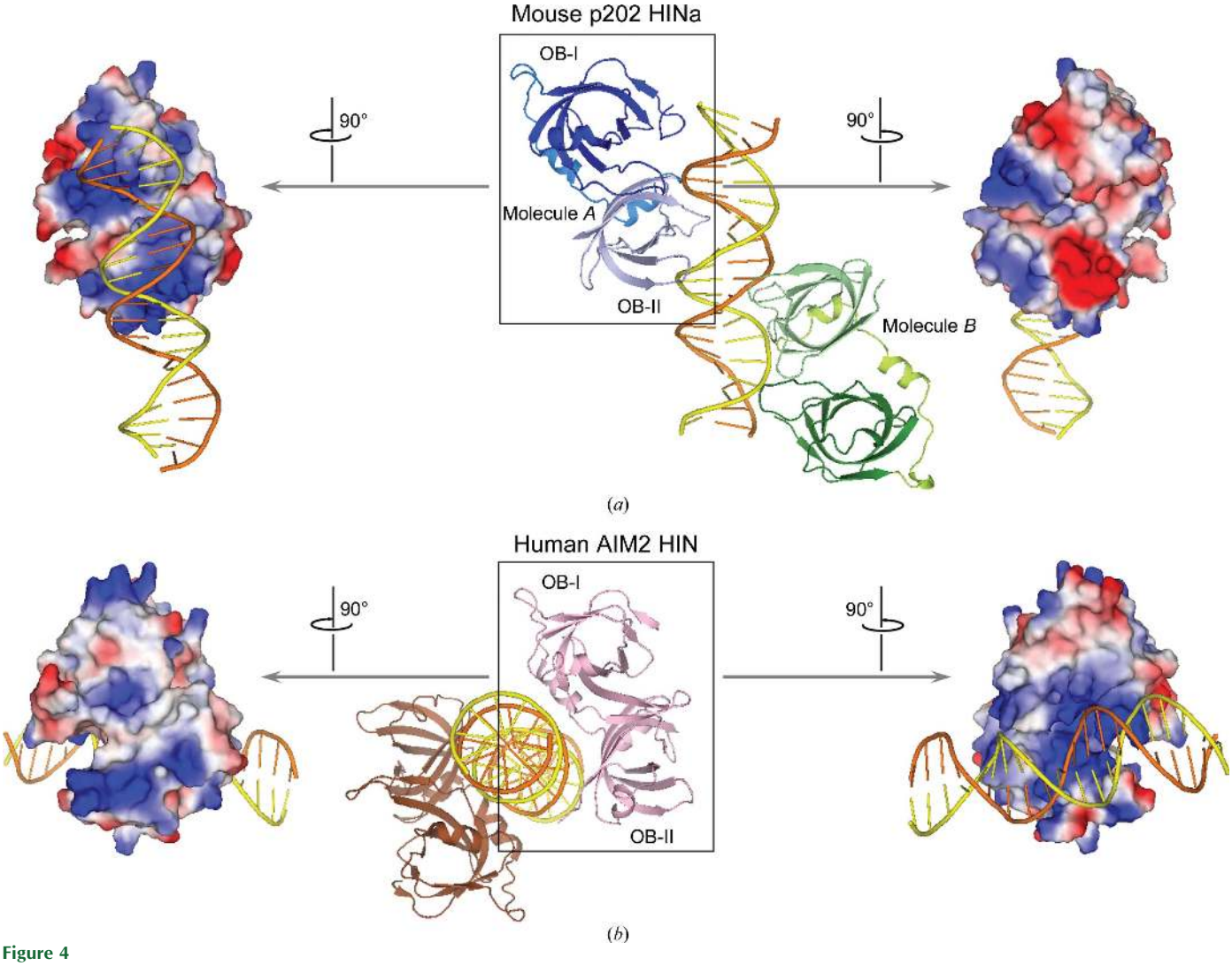

Figure 4
p202 HINa and AIM2 HIN bind to dsDNA using completely different interfaces. Molecule *A* of p202 HINa is positioned in the same orientation as one of the AIM2 HIN molecules (megenta) in the AIM2 HIN–dsDNA structure (PDB entry 3rn2). (*a*) The DNA-binding interface (left) and its opposite surface (right) in p202 HINa. The left and right panels show surface representations of molecule *A* (coloured according to electrostatic potential: positive, blue; negative, red) in views related to the middle ribbon diagram by 90° clockwise or anticlockwise rotations around a vertical axis. (*b*) The DNA-binding interface (right) and its opposite surface (left) in AIM2 HIN. The two AIM2 HIN molecules bound to dsDNA within the asymmetric unit are coloured pink and brown, respectively, and the surface representations are generated from the boxed AIM2 HIN molecule.

corresponding I-loop$_{1,2}$ and I-loop$_{4,5}$ regions of the p202 HINa OB-I fold are also largely positively charged. This basic surface is close to the DNA backbone, but makes little direct contact. However, the basic region of the OB-II fold of AIM2 HIN is located differently

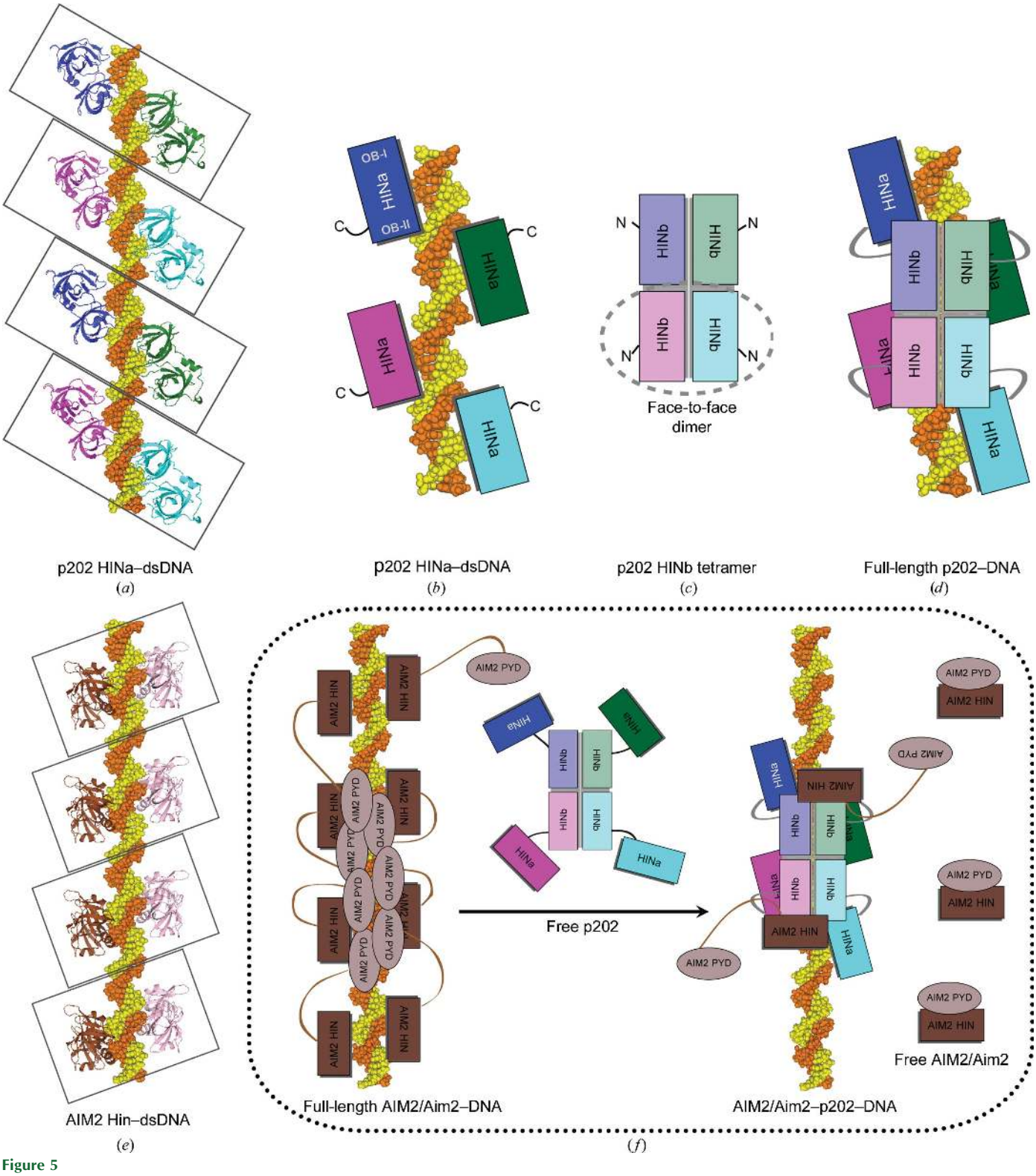

Figure 5
Binding of p202 to DNA prevents the formation of the AIM2/Aim2 inflammasome. (*a*) Crystal packing of the p202 HINa–dsDNA complex. Four asymmetric units indicated by black boxes are shown with their dsDNA chains forming a pseudo-duplex. (*b*) Schematic model of four adjacent p202 HINa molecules bound to dsDNA. (*c*) Schematic model of the p202 HINb tetramer observed in the crystal structure (PDB entry 4l5t). (*d*) Schematic model of full-length p202 binding to DNA. The p202 HINb tetramer tethers four HINa domains together, which in turn bind to dsDNA simultaneously. (*e*) Crystal packing of the AIM2 HIN–dsDNA complex (PDB entry 3rn2). (*f*) Model of the negative regulation of AIM2/Aim2 signalling by p202. The HIN domain of AIM2/Aim2 binds to dsDNA, which leads to the oligomerization of its PYD domain. The p202 HINa domain competes with AIM2/Aim2 HIN for DNA binding, while the p202 HINb tetramer recruits the released AIM2/Aim2 HIN to two opposite ends.

from that of p202 HINa, and the corresponding surface of the AIM2 HIN OB-I fold is largely hydrophobic (Fig. 4*b*, left panel). This observation is consistent with the fact that this side of the AIM2 HIN domain cannot bind DNA. Indeed, the AIM2 HIN domain binds vertically to the DNA molecule through a concave basic surface formed by residues from both OB folds and the linker between them (Figs. 4*b* and 2*d*). Instead, the corresponding surface of the p202 HINa molecule is dominated by a negatively charged region formed by Glu211, Asp214 and Glu243, which would clearly exclude the binding of a DNA molecule (right panel of Fig. 4*a* and Fig. 2*d*). Significantly, although the sequence identities between p202 HINa, IFI16 HINb and AIM2 HIN are 40–50%, their basic residues involved in nonspecific interactions with the DNA backbones are clearly different. The DNA-binding residues in the AIM2 HINc domain, Lys160, Lys162, Lys163, Lys204 and Arg311, are substituted by Thr68, Thr70, Glu71, Asn110 and Gln217 in the p202 HINa domain, and the key interacting residues of p202 HINa, Ser166, Lys180, Thr187, Lys198, His222 and Arg224, are replaced by Leu260, Thr274, Leu281, Glu292, Thr316 and Ser318 in the AIM2 HIN domain (Fig. 2*d*). Therefore, despite the high sequence identity and conserved conformation of all determined HIN domains, the p202 HINa domain binds to dsDNA *via* a distinct interface from those of the AIM2 HIN and IFI16 HINb domains (Jin *et al.*, 2012).

3.4. Functional implications

The rapid development of X-ray crystallography had greatly benefited our understanding of the interaction between the DNA-binding proteins and their specific DNA sequences. In many reported protein–DNA complex structures, the DNA molecules from adjacent asymmetric units pack end-to-end and form pseudo-continuous double helices that match the helical repeat of the regular B-DNA. In such cases, the protein–DNA interactions observed in the crystal structures most likely represent the DNA-recognition modes under physiological conditions. In our p202 HINa–DNA co-crystals, the dsDNA molecules indeed form pseudo-continuous duplexes through head-to-tail packing, with the p202 HINa domains decorated along dsDNA with one HIN domain spanning more than 10 bp on one side of the DNA duplex (Fig. 5*a*). Moreover, a similar packing mode is observed in the crystals of AIM2 HIN in complex with the same dsDNA (Fig. 5*e*), although AIM2 binds dsDNA through an interface on the opposite side of that used by p202 HINa (Jin *et al.*, 2012).

Two recent structural studies of dsDNA recognition by p202 have also demonstrated highly similar interactions between the p202 HINa domain and dsDNA (Ru *et al.*, 2013; Yin *et al.*, 2013). However, in the two reported p202 HINa–dsDNA structures (PDB entries 4jbk and 4l5s), the p202 HINa protein binds at one end of the DNA molecule (14 and 10 bp/12-mer, shorter than the 20 bp dsDNA that we used in crystallization trials) and thus mediates the end-to-end packing of DNA. In the third complex structure (PDB entry 4l5r), only one molecule of the p202 HINa protein was shown to recognize the middle portion of an 18 bp dsDNA that was generated from a 20-mer oligonucleotide with a two-nucleotide overhang at the 3′ end. Notably, this overhang was unable to pair up and there did not seem to be head-to-tail packing of DNA molecules. Therefore, the choice of DNA and its length and sequence can be critical to the molecular mechanism of the protein–DNA interaction and the DNA packing mode.

Interestingly, the full-length p202 protein and its second HIN domain (p202 HINb) have been shown to tetramerize (Yin *et al.*, 2013). In the structure of p202 HINb alone, two molecules form a face-to-face dimer *via* the same interface that p202 HINa uses to bind dsDNA, and two such dimers further oligomerize end to end (Fig. 5*c*). The four N-termini in the p202 HINb tetramer all point outwards, and the C-termini of the p202 HINa domains in our complex structure are located distal to the dsDNA (Fig. 5*b*). These observations enable the connection between two HIN domains *via* a flexible linker of 10–20 residues. With the information from the crystal packing of the p202 HINa–dsDNA complex, we propose a model of how the full-length p202 protein binds dsDNA (Fig. 5*d*). Four p202 HINb domains form a tetramer, which tethers four p202 HINa domains in close proximity. This would allow the simultaneous binding of four p202 HINa domains to a dsDNA molecule as in the protein–DNA co-crystals.

How then does p202 negatively regulate AIM2/Aim2 signalling? AIM2/Aim2-mediated inflammatory signalling is highly conserved in human and mouse (Choubey, 2012). Initiation of this pathway requires a long DNA duplex as an oligomerization platform that recruits multiple human AIM2 or mouse Aim2 proteins (Fig. 5*e*). The HIN domains of human AIM2 and mouse Aim2 are highly conserved (Fig. 2*d*), and structural studies showed that they bind to dsDNA in a similar mode (Jin *et al.*, 2012; Ru *et al.*, 2013). Recently, Yin and coworkers found that the p202 HINb domain directly binds AIM2 HIN and thereby simulated a docking model (Yin *et al.*, 2013). In this model, two AIM2 HIN domains bind at both ends of the p202 HINb tetramer and are spatially separated, which would prevent AIM2-mediated ASC oligomerization and further signal tranduction. In addition to this mechanism, we believe that the competition of p202 HINa with AIM2/Aim2 for DNA binding might also play a role in the inhibition of AIM2 function (Ru *et al.*, 2013). Firstly, our DNA-binding analyses indicate that p202 HINa binds dsDNA approximately fivefold more tightly than human AIM2 HIN and mouse Aim2 HIN (Fig. 1*a*), which is consistent with the structural observation that each p202 HINa domain buries a larger surface area of DNA than AIM2 HIN ($\sim$1370 *versus* $\sim$1150 Å^2). In addition, p202 exists as a tetramer with the four p202 HINa domains simultaneously binding the same DNA duplex, which further strengthens the interaction of p202 with DNA. When the tetrameric p202 competes for dsDNA that is bound by AIM2, the p202 HINa domain with higher DNA-binding affinity can displace AIM2/Aim2 HIN from DNA (Fig. 5*f*). The free AIM2/Aim2 HIN domain could then be recruited to the closely linked p202 HINb tetramer, which would prevent the re-binding of AIM2/Aim2 HIN to DNA. Therefore, both the competition of p202 HINa for DNA binding and the direct interaction of p202 HINb with AIM2/Aim2 HIN are required for effective inhibition of the AIM2 inflammasome formation.

In conclusion, we determined the structure of two p202 HINa molecules in complex with a DNA duplex *via* nonspecific interactions. In the protein–DNA co-crystals the DNA molecules pack head-to-tail into pseudo-continuous double helices, while the proteins decorate both sides of the DNA duplex. Together with the tetramerization of the p202 HINb domain and its recruitment of AIM2 HIN, we propose a conceivable model of the complex between full-length p202 and dsDNA which sheds light on the mechanism of the inhibition of Aim2 signalling by p202.

We thank the staff of beamline 17U at the Shanghai Synchrotron Radiation Facility (SSRF) for assistance in data collection and Dr Lei Chen, Chuangye Yan and Shu-Tao Xie for crystal optimization and structural refinement. This work was supported in part by grant 31070643 from the Natural Science Foundation of China and grant 20121080028 from Tsinghua University.

References

Adams, P. D. *et al.* (2010). *Acta Cryst.* D**66**, 213–221.

Akira, S., Uematsu, S. & Takeuchi, O. (2006). *Cell*, **124**, 783–801.

Barbalat, R., Ewald, S. E., Mouchess, M. L. & Barton, G. M. (2011). *Annu. Rev. Immunol.* **29**, 185–214.

Bürckstümmer, T., Baumann, C., Blüml, S., Dixit, E., Dürnberger, G., Jahn, H., Planyavsky, M., Bilban, M., Colinge, J., Bennett, K. L. & Superti-Furga, G. (2009). *Nature Immunol.* **10**, 266–272.

Chen, V. B., Arendall, W. B., Headd, J. J., Keedy, D. A., Immormino, R. M., Kapral, G. J., Murray, L. W., Richardson, J. S. & Richardson, D. C. (2010). *Acta Cryst.* D**66**, 12–21.

Choubey, D. (2012). *Clin. Immunol.* **142**, 223–231.

Choubey, D. & Gutterman, J. U. (1996). *Biochem. Biophys. Res. Commun.* **221**, 396–401.

Choubey, D., Walter, S., Geng, Y. & Xin, H. (2000). *FEBS Lett.* **474**, 38–42.

Dawson, M. J. & Trapani, J. A. (1996). *J. Leukoc. Biol.* **60**, 310–316.

Dombrowski, Y., Peric, M., Koglin, S., Kammerbauer, C., Göss, C., Anz, D., Simanski, M., Gläser, R., Harder, J., Hornung, V., Gallo, R. L., Ruzicka, T., Besch, R. & Schauber, J. (2011). *Sci. Transl. Med.* **3**, 82ra38.

Emsley, P. & Cowtan, K. (2004). *Acta Cryst.* D**60**, 2126–2132.

Fang, R., Tsuchiya, K., Kawamura, I., Shen, Y., Hara, H., Sakai, S., Yamamoto, T., Fernandes-Alnemri, T., Yang, R., Hernandez-Cuellar, E., Dewamitta, S. R., Xu, Y., Qu, H., Alnemri, E. S. & Mitsuyama, M. (2011). *J. Immunol.* **187**, 4890–4899.

Fernandes-Alnemri, T., Yu, J.-W., Datta, P., Wu, J. & Alnemri, E. S. (2009). *Nature (London)*, **458**, 509–513.

Fernandes-Alnemri, T., Yu, J.-W., Juliana, C., Solorzano, L., Kang, S., Wu, J., Datta, P., McCormick, M., Huang, L., McDermott, E., Eisenlohr, L., Landel, C. P. & Alnemri, E. S. (2010). *Nature Immunol.* **11**, 385–393.

Ge, J., Gong, Y.-N., Xu, Y. & Shao, F. (2012). *Proc. Natl Acad. Sci. USA*, **109**, 6193–6198.

Hornung, V., Ablasser, A., Charrel-Dennis, M., Bauernfeind, F., Horvath, G., Caffrey, D. R., Latz, E. & Fitzgerald, K. A. (2009). *Nature (London)*, **458**, 514–518.

Jin, T., Perry, A., Jiang, J., Smith, P., Curry, J. A., Unterholzner, L., Jiang, Z., Horvath, G., Rathinam, V. A., Johnstone, R. W., Hornung, V., Latz, E., Bowie, A. G., Fitzgerald, K. A. & Xiao, T. S. (2012). *Immunity*, **36**, 561–571.

Jones, J. W., Kayagaki, N., Broz, P., Henry, T., Newton, K., O'Rourke, K., Chan, S., Dong, J., Qu, Y., Roose-Girma, M., Dixit, V. M. & Monack, D. M. (2010). *Proc. Natl Acad. Sci. USA*, **107**, 9771–9776.

Kersse, K., Verspurten, J., Vanden Berghe, T. & Vandenabeele, P. (2011). *Trends Biochem. Sci.* **36**, 541–552.

Kerur, N., Veettil, M. V., Sharma-Walia, N., Bottero, V., Sadagopan, S., Otageri, P. & Chandran, B. (2011). *Cell Host Microbe*, **9**, 363–375.

Kim, S., Bauernfeind, F., Ablasser, A., Hartmann, G., Fitzgerald, K. A., Latz, E. & Hornung, V. (2010). *Eur. J. Immunol.* **40**, 1545–1551.

Koning, H. D. de, Bergboer, J. G., van den Bogaard, E. H., van Vlijmen-Willems, I. M., Rodijk-Olthuis, D., Simon, A., Zeeuwen, P. L. & Schalkwijk, J. (2012). *Exp. Dermatol.* **21**, 961–964.

Laskowski, R. A., MacArthur, M. W., Moss, D. S. & Thornton, J. M. (1993). *J. Appl. Cryst.* **26**, 283–291.

Liao, J. C. C., Lam, R., Brazda, V., Duan, S., Ravichandran, M., Ma, J., Xiao, T., Tempel, W., Zuo, X., Wang, Y.-X., Chirgadze, N. Y. & Arrowsmith, C. H. (2011). *Structure*, **19**, 418–429.

Ludlow, L. E., Johnstone, R. W. & Clarke, C. J. (2005). *Exp. Cell Res.* **308**, 1–17.

McCoy, A. J., Grosse-Kunstleve, R. W., Adams, P. D., Winn, M. D., Storoni, L. C. & Read, R. J. (2007). *J. Appl. Cryst.* **40**, 658–674.

Otwinowski, Z. & Minor, W. (1997). *Methods Enzymol.* **276**, 307–326.

Park, H. H. (2012). *Apoptosis*, **17**, 1247–1257.

Park, H. H., Lo, Y.-C., Lin, S.-C., Wang, L., Yang, J. K. & Wu, H. (2007). *Annu. Rev. Immunol.* **25**, 561–586.

Rathinam, V. A., Jiang, Z., Waggoner, S. N., Sharma, S., Cole, L. E., Waggoner, L., Vanaja, S. K., Monks, B. G., Ganesan, S., Latz, E., Hornung, V., Vogel, S. N., Szomolanyi-Tsuda, E. & Fitzgerald, K. A. (2010). *Nature Immunol.* **11**, 395–402.

Roberts, T. L., Idris, A., Dunn, J. A., Kelly, G. M., Burnton, C. M., Hodgson, S., Hardy, L. L., Garceau, V., Sweet, M. J., Ross, I. L., Hume, D. A. & Stacey, K. J. (2009). *Science*, **323**, 1057–1060.

Ru, H., Ni, X., Zhao, L., Crowley, C., Ding, W., Hung, L.-W., Shaw, N., Cheng, G. & Liu, Z.-J. (2013). *Cell Res.* **23**, 855–858.

Saiga, H., Kitada, S., Shimada, Y., Kamiyama, N., Okuyama, M., Makino, M., Yamamoto, M. & Takeda, K. (2012). *Int. Immunol.* **24**, 637–644.

Sauer, J. D., Witte, C. E., Zemansky, J., Hanson, B., Lauer, P. & Portnoy, D. A. (2010). *Cell Host Microbe*, **7**, 412–419.

Schattgen, S. A. & Fitzgerald, K. A. (2011). *Immunol. Rev.* **243**, 109–118.

Sung, M. W., Watts, T. & Li, P. (2012). *Acta Cryst.* F**68**, 1081–1084.

Tsuchiya, K., Hara, H., Kawamura, I., Nomura, T., Yamamoto, T., Daim, S., Dewamitta, S. R., Shen, Y., Fang, R. & Mitsuyama, M. (2010). *J. Immunol.* **185**, 1186–1195.

Winn, M. D. *et al.* (2011). *Acta Cryst.* D**67**, 235–242.

Yin, Q., Sester, D. P., Tian, Y., Hsiao, Y.-S., Lu, A., Cridland, J. A., Sagulenko, V., Thygesen, S. J., Choubey, D., Hornung, V., Walz, T., Stacey, K. J. & Wu, H. (2013). *Cell Rep.* **4**, 327–339.